Virology 403 (2010) 137–144

Contents lists available at ScienceDirect

Virology

journal homepage: www.elsevier.com/locate/yviro

Pathogenesis of *Junonia coenia* densovirus in *Spodoptera frugiperda*: A route of infection that leads to hypoxia

Doriane Mutuel [a], Marc Ravallec [a], Beatrice Chabi [b], Cecilia Multeau [a,c], Jean-Michel Salmon [d], Philippe Fournier [a], Mylène Ogliastro [a,*]

[a] INRA, UMR 1231, F-34000 Montpellier, France
[b] INRA, UMR 866, F-34000 Montpellier, France
[c] BIOTOP 06560, Valbonne, France
[d] INRA, UMR 1083, F-34000 Montpellier, France

ARTICLE INFO

Article history:
Received 15 January 2010
Returned to author for revision
16 February 2010
Accepted 3 April 2010
Available online 10 May 2010

Keywords:
Insect parvovirus
Densovirus
Host range
Spodoptera frugiperda
Biological control
Pathogenesis
Tissue tropism
Anoxia
ROS
Insect trachea

ABSTRACT

To evaluate densovirus potential against lepidopteran pests and their capacity to invade new hosts, we have characterised *in vivo* the infection and pathogenesis of the *Junonia coenia* densovirus (*Jc*DNV) in the noctuid pest *Spodoptera frugiperda*. Here we show that infection starts with the ingestion of viral particles that cross the midgut epithelium without replicating. By quantitative PCR we established the kinetic and the route of infection, from virus ingestion to replication in visceral tracheae and hemocytes. *Jc*DNV has a high particle-to-infection ratio mostly due to the barrier function of the midgut. Pathology and cytopathology suggested that infection of tracheal cells impairs oxygen delivery to demanding tissues leading to cytopathic effects in all the tissues. Finally, larval death results from several physiological shocks, including molting arrest and anoxia.

Introduction

Densoviruses (DNVs) were first discovered as the causative agents of natural epizootics in populations of the greater waxmoth, *Galleria mellonella* (Meynadier et al., 1964). The pathology associated with the disease described a "cellular dense nucleosis", giving their first name to these viruses. Since then, similar epizootics have been discovered in other insects, lepidoptera, mosquitoes, and coackroaches (Hu et al., 1994; Meynadier et al., 1964; O'Neill et al., 1995; Rivers and Longworth, 1972). Because of their high virulence and efficient transmission among insect pests and disease-vectors, DNVs were considered as biological control agents. However their use for this purpose has been under-considered mainly due to the overpromotion of chemical pesticides and the lack of investments. As a consequence, the knowledge on DNV pathogenesis and host range remained globally poor. Nowadays, the development of insect resistance and eco-aware societal demand further complicate pest management. Alternative strategies, including the use of viral agents, have to be constantly renewed and investigated; in this context DNVs are reconsidered with interest.

DNVs are small icosaedral and non-enveloped viral particles (25 nm), packaging a 6 kb linear single-stranded DNA genome ended by two hairpin structures. These characteristics make these insect viruses belong to *Parvoviruses*. Due to their arthropod host range, they have been grouped further in the *Densovirinae* subfamily, including *Densovirus*, *Pefudensovirus*, *Iteravirus* and *Brevidensovirus* genera. Today, more than thirty *Densovirinae* have been discovered, infecting at least 5 insect orders. They reveal a great diversity not only in genomic structures and sequences but also in the biology of infection and host range (Bergoin and Tijssen, 2008). Although transmission mechanisms are poorly known, infection proceeds through oral contamination; the virus spread horizontally in the population and infection is often associated with a high virulence as illustrated by epizootics (Rivers and Longworth, 1972; Meynadier et al., 1964). Interestingly, vertical transmission has been also observed for aphid and mosquito densoviruses associated with low virulence and high replication (van Munster et al., 2003). Vertical transmission

* Corresponding author. Mailing address: Biologie Intégrative et Virologie des Insectes UMR, 1231 INRA-Université Montpellier II, Place Eugène Bataillon, Bat. 24, cc101, 34095 Montpellier Cedex 5, France. Fax: +33 467 144 299.
E-mail address: ogliastr@supagro.inra.fr (M. Ogliastro).

0042-6822/$ – see front matter © 2010 Elsevier Inc. All rights reserved.
doi:10.1016/j.virol.2010.04.003

allowed exploring an alternative use as expression or transducing vectors (Carlson et al., 2006; Ren et al., 2008).

To evaluate the suitability of using DNVs in lepidopteran pest control, and assess for their capacity and their risks of invading new hosts, mechanisms underlying specificity and pathogenesis need to be deciphered carefully. Densoviruses are named according to the first host name they have been discovered on, which does not account for their host range. Among closely related DNVs, host spectrum can be restricted to one host, as described for the *G. mellonella* (*Gm*) DNV, or be rather large and includes several host species, as mentioned for the *Junonia coenia* (*Jc*) DNV or the maize worm *Mythimna loreyi* (*Ml*) DNV (Fediere et al., 2004). Although few data exist, a diversity of tissue tropism has also been described. Some densoviruses infect only the midgut whereas others have a broad tissue tropism but except the midgut, as described for *Gm*DNV (Bergoin and Bres, 1968).

The densovirus prototype, *J. coenia* (*Jc*) DNV was first discovered on a nymphalid and had been propagated on different lepidopteran species including the noctuid *Mamestra brassicae* (Rivers and Longworth, 1972). More recently, *Jc*DNV was shown to be lethal for *Spodoptera littoralis* following intrahemocoelic injections although virus injections might only partially reflect the host range (Abd-Alla et al., 2004; Barat-Houari et al., 2006; Vendeville et al., 2009).

In this work, we analysed the *in vivo* *Jc*DNV infection and pathogenesis in the agronomical pest, the fall armyworm *Spodoptera frugiperda*, from oral contamination to death. We established that *Jc*DNV is pathogenic for *Spodoptera* species and that viral replication occurred in different tissues but excluded the midgut. We showed that the *Jc*DNV pathogenesis severely affects epidermis and tracheae inducing molting failure and oxidative stress. Infection finally leads to anoxia and death of the larvae.

Results

S. frugiperda is susceptible to JcDNV oral infection: effects on development and growth

Larval stages are a period of intense feeding and rapid growth. In the rearing conditions, *S. frugiperda* caterpillars undergo 6 larval stages, growing in about 2 weeks, from 1 mm and 0.5 mg to more than 3 cm and 0.8 g. To assess for the *S. frugiperda* larval susceptibility to *Jc*DNV we conducted oral infection bioassays. Cohorts of 24 individuals at the second larval instars (L2) were fed with food contaminated with serial dilutions of purified *Jc*DNV. Initial virus concentration was estimated by quantitative PCR according to a *Jc*DNV standard curve at 2.5×10^{14} viral genomes (vg)/ml. Mortality of virus fed L2 increased linearly with increasing viral concentration, showing that infection was dose dependent (Fig. 1A). The lethal dose (LD) required to kill 50% of the cohorts (LD_{50}) at L2 was estimated at 5×10^{9} viral genomes (vg) and defined one LD_{50} as the unit used in this study. Decreasing the viral dose to 0.05 LD_{50} did not affect metamorphosis but strongly impaired the pupal development since only 20% of infected larvae developed until the adult stage. This delayed mortality showed that infection and pathogenesis were also time-dependent. In order to analyse whether *Jc*DNV could cause subliminal infections in *S. frugiperda*, we performed quantitative PCR analysis of chrysalids or adults that survived to infection. We were not able to detect any JcDNV suggesting that infection is probably cleared during metamorphosis (data not shown).

Similar results were obtained after *per os* contamination of *S. littoralis*. Interestingly this species was 100-fold more resistant than *S. frugiperda* to *Jc*DNV infection (unpublished data).

To further characterise *Jc*DNV virulence, two phenotypic traits of infection were analysed, time to death and larval weight uptake. L2 to L5 larval cohorts were infected with 100 LD_{50}, an over dose previously estimated to kill 100% of infected L2 at larval stage. All larvae were weighted every day to death. Results presented in Fig. 1B showed that for L2 infected larvae, the effect of infection on weight uptake was observed within a day of death meaning that infected larvae maintained their feeding until late in infection. Similar results were obtained with L3 except that infection time was increased and larval death occurred between 6 and 9 days. Concerning L4 and L5 infected with the same dose, death occurred between 7 and 12 days, before or at metamorphosis; larvae often displayed a half-pupa phenotype (data not shown) with no effect on larval weight uptake due to the natural cessation of feeding preceding metamorphosis in control larvae (Fig. 1C).

To estimate whether the lethal dose depends on the developmental stage at the time of infection we next compared the *Jc*DNV lethal doses required at early (L2) and late (L5) larval instars to cause death either at larval stage (Larval) or during metamorphosis, impairing the adult development (Adult). As shown in Fig. 1C, 100 LD_{50} were required to kill 50% of L5 larvae before metamorphosis and might be correlated with the larval mass increase between L2 and L5. This 100-fold difference was balanced by extending the time of infection: considering mortality at pupal stage, 1 LD_{50} and 10 LD_{50} respectively killed 80% of L2 and L5.

Since *Jc*DNV infection affected the development depending on the dose, we next assessed whether infection affected larval molting. A cohort of newly molted third instar (L3) larvae were orally infected with different *Jc*DNV doses, from low (0.01 LD_{50}) to high doses (100 LD_{50}). Molts were estimated by counting the head capsules in each cohort every day to pupal molt (1 capsule per molt). As shown in Fig. 1D, the number of molts decreased when *Jc*DNV concentration increased. Most L3 larvae infected with 100 LD_{50} molted to the 4th instar and then stopped molting. At low viral dose (0.01 LD_{50}), no significant effect on molting was observed, compared to the control cohort. These results showed that molting failure was also dose dependent.

JcDNV pathogenesis and time course of infection in S. frugiperda

To investigate the pathogenesis of *Jc*DNV, we next explored the tissue tropism and the cytopathology induced by *Jc*DNV ingestion. Caterpillars infected at L2 stage with 100 LD_{50} were harvested 5 days pi and analysed by whole mount immuno-labelling with an anti-*Jc*DNV antibody (Fig. 2). Microscopic observations showed a strong labelling in visceral muscles, epidermis and tracheal cells (Fig. 2A, panels 1–3′); all cells displayed “dense nuclei”, hallmark of densonucleosis. Among hemocytes populations, labelled and spread on a coverslip, a productive infection was only observed in one cell type, morphologically identified as granulocytes by phase contrast (Fig. 2A, panels 4–5′). Densonucleosis was also observed in hindgut and foregut cells (data not shown) but not in midgut cells (Fig. 2A, panels 6–6′). No densonucleosis was observed in fat body or in malpighian tubules where only the tracheae branching on these tissues were labelled (Fig. 2A, panels 7–7′). Electron microscopy (TEM) analysis confirmed the presence of viral particles in the hypertrophied nucleus of these cells (Fig. 2B, panels 1–5). Severe defects in epidermis sections were observed, with cuticle disorganisation, numerous autophagic-like vacuoles and pseudo-crystalline viral arrangements in the cytoplasm (Fig. 2B, panels 1–2). Similar disorganisation affected tracheal cells, viral particles were observed within vesicles and within the basal lamina (Fig. 2B, panels 3–4). No pseudo-crystalline viral arrangement was observed. In some tracheae, electron-dense material together with virus-like aggregates obstructed the lumina (panel 5), that might be accumulated chitin that have not been eliminated before hatching. No *Jc*DNV was detected in midgut cells nuclei or in nervous system cells and locomotion muscles. In malpighian tubules and fat body, very seldom viral foci could be observed, closely associated with tracheae, although cytopathies were observed in all these cells (Fig. 2C). In fat body, cells presented shrunk nucleus and numerous autophagic- and apoptic-like bodies were observed in the

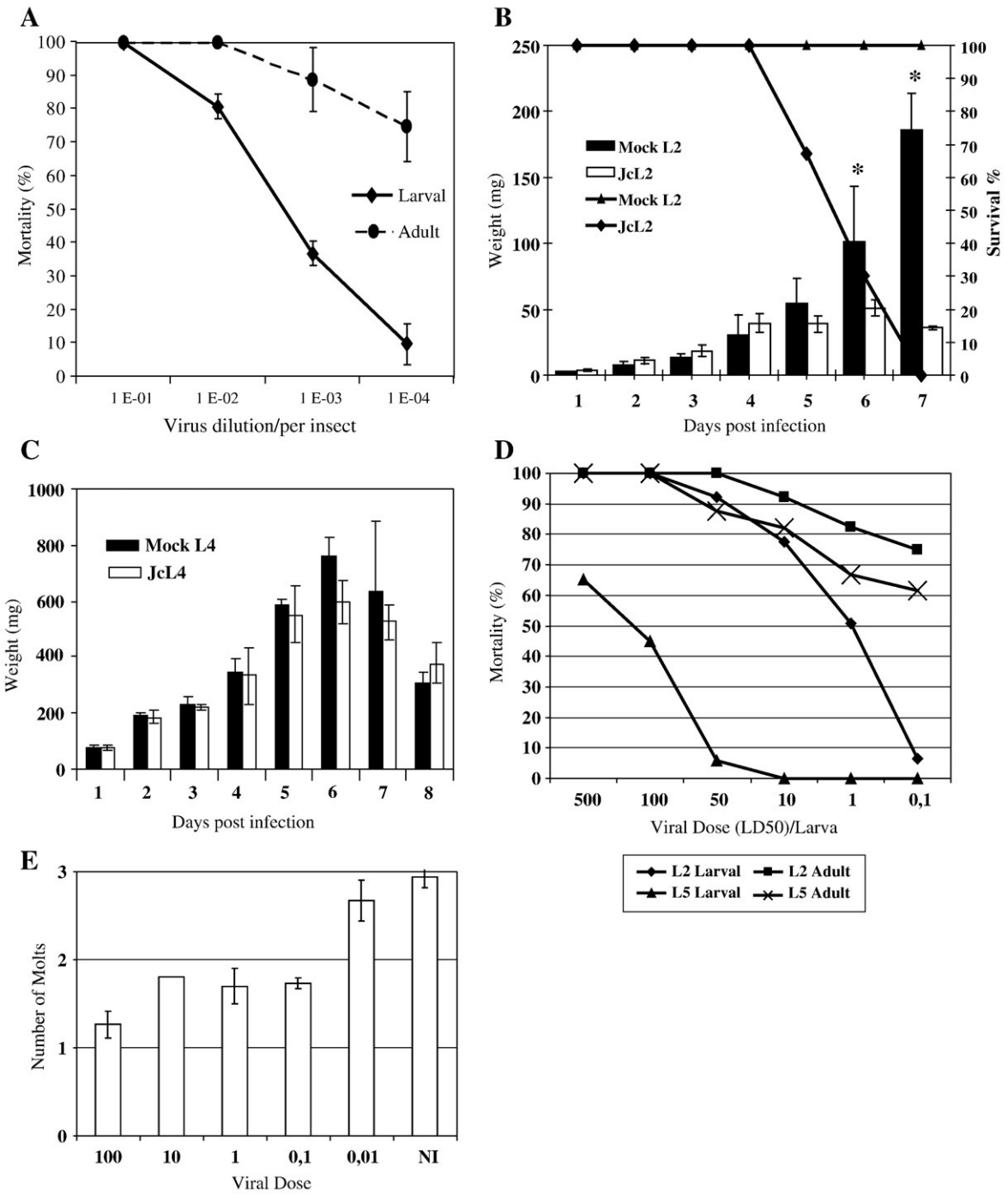

Fig. 1. Effects of oral infections of *S. frugiperda* with *Jc*DNV (A) lethal dose 50 (LD_{50}) determination after second instar larvae (L2) oral infections. Mortality levels were determined after infection with increasing *Jc*DNV concentrations at pre- (Larval) and post-metamorphosis (Adult). Viral dosages were determined by real time qPCR according to a *Jc*DNV standard curve. Larvae ($n=24$) were infected and the percent mortality was calculated at each concentration by dividing the number of deaths at each developmental stage (Larval and Adult) by the number of larvae infected. (B–C) Weight uptake and percent of larval survival (1% mortality) after L2 (B) and L4 (C) infections with 100 LD_{50} ($n=30$). (D) Larval and adult lethal dose determinations after L2 and L5 infections with increasing *Jc*DNV concentrations ($\times LD_{50}$). (E) Number of larval molts after infections of newly molted L3 with increasing *Jc*DNV doses ($\times LD_{50}$). Head capsules were counted every day to metamorphosis or death ($n=30$). Number of molts was estimated by dividing the number of head capsules at each dose by the total number of larvae in each cohort ($n=30$).

cytoplasm (Fig. 2C, panels 1–2). Darken space between cells was filled with electron-dense material compared to mock-infected cells. Similar ultra structural defects were observed in midgut cells displaying highly damaged apical brush borders and "opened" junctions with many lipidic and autophagic-like vesicles accumulated within the cytoplasm (Fig. 2C, panel 3). At this time pi, no DNA replication was observed in intestinal cells, as suggested by BrdU incorporation experiment (Fig. 2C, panels 4–5), suggesting that no midgut cell renewal occurred anymore in infected larvae compared to stage-matched control mock-infected larvae.

We next sought to understand the time course and the route of *Jc*DNV infection from oral contamination to dissemination within the host. Infection starts with the ingestion of viral particles. To reach the replicative tissues described above, the virus must first cross the protective peritrophic membrane lining the midgut and the midgut epithelium, circumventing cell nucleus. Visceral tracheae and

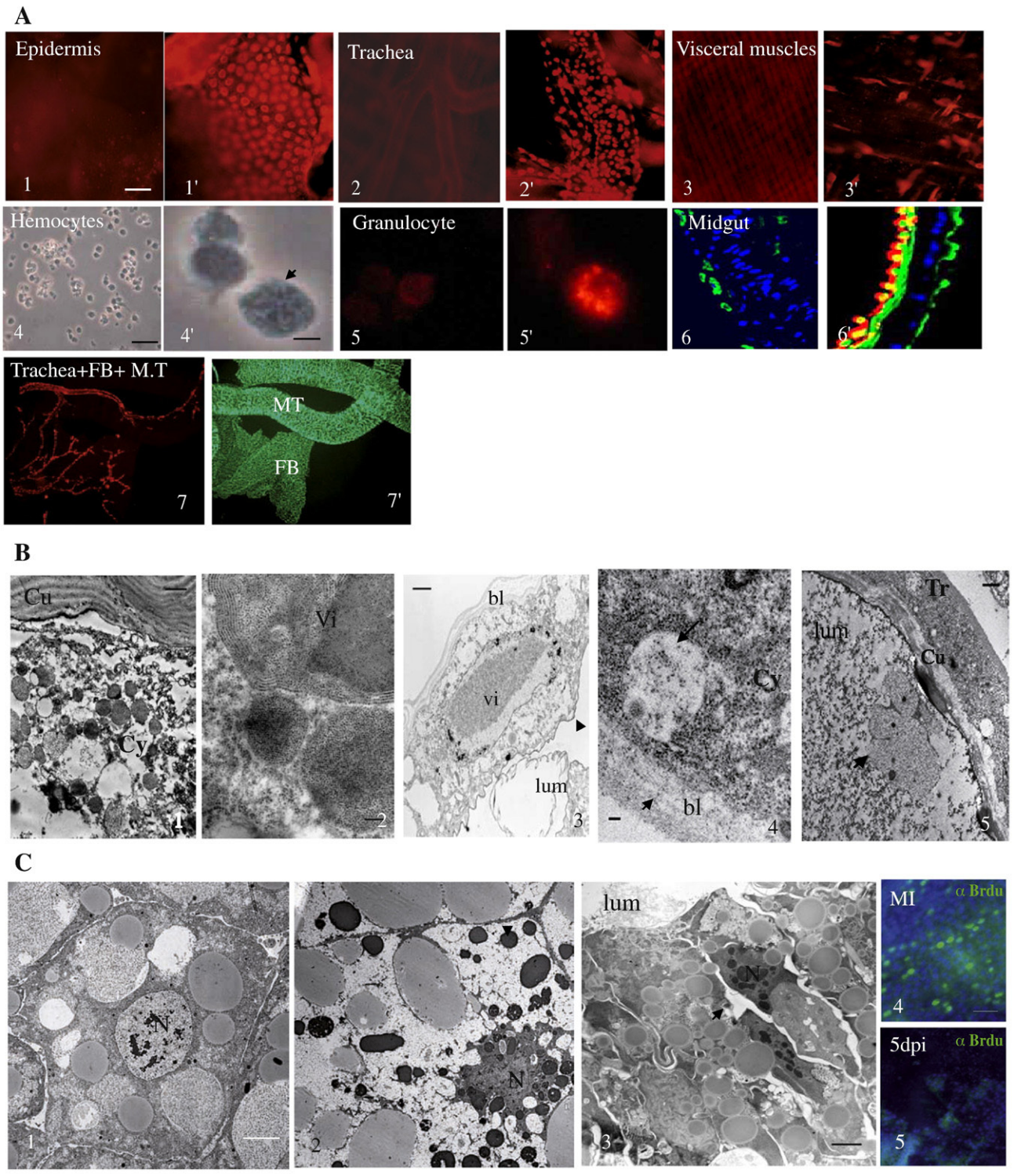

Fig. 2. *Jc*DNV tissue tropism and pathogenesis. L2 were infected and dissected 5 days pi. (A) Mock-infected (1–7) and infected (1′–7′) larvae were dissected and immunocytochemistry was performed on whole mounts of the different tissues, or on cryosections for the midgut. *Jc*DNV labelling (in red), nuclei (in blue) and cortical actin staining (in green, 6–6′) were analysed by fluorescence microscopic. In the infected midgut cryosection, visceral muscles labelling (yellow) resulted from the superimposition of JcDNV (red) and actin (green). Hemocytes were analysed by phase contrast (4–4′) and fluorescence (5–5′) showing that only granulocytes were infected. Scale bars (1–3′) 0.15 mm, (4) 50 µm, (4′–6′) 5 µm, and (7–7′) 0.5 mm. (B) TEM analysis of ultrathin sections. Epidermis, scale bars 2 µm (1), 250 nm (2). Tracheal cells (3–5). Arrowhead indicates tracheal cuticle. (4–5) Arrows indicate viral particles within vesicle, basal lamina and viral like particles within the lumen of a trachea. Scale bar, 2 µm. (C) TEM analysis of fat body cells from mock-infected (1) and infected larvae (2) and midgut cells from infected larva (3). Scale bars, 2 µm. Midgut cell DNA replication after 24 h BrdU injection within mock-infected (4) or 5-day infected larvae (5). Nuclei were labelled with DAPI (blue) and BrdU positive cells were labelled with anti-BrdU antibody (green). bl, basal lamina; Cu, cuticle; Cy, cytoplasm; lum, lumina; tr, trachea; vi, virus.

hemocytes directly contact midgut cells and are permissive to *Jc*DNV replication. We assumed that the time for *Jc*DNV to infect these cells would more or less reflect the time for viral particles to cross the midgut. To seek for *Jc*DNV accumulation within midgut, hemocytes and trachea, we used real time quantitative PCR to analyse the kinetic of infection of these cells. Ten L4 larvae per condition were

individually fed with 100 LD_{50} of *Jc*DNV and kept isolated with fresh food in clean plates. Four instar larvae were used for this experiment because their size allows an easy dissection. Ten larvae were similarly mock-infected as control for each time point. At different times post ingestion, larvae were thoroughly washed and hemocytes, visceral tracheae or midgut cells were collected by bleeding or dissection to extract total DNA. Simultaneous determinations of viral and cellular DNA quantities were performed by quantitative PCR using specific viral and cellular primers to consider the relative viral genome build-up per cell (calculated by the ΔΔCt method). Results showed that *Jc*DNV was detected in both hemocytes and trachea at 4 h pi but not in isolated midgut cells (Fig. 3A). Intriguingly, between 4 and 48 h pi, a viral clearance followed by a relative latency occurred in hemocytes and tracheae while in midgut cells, a relative significant amount of *Jc*DNV was detected at 16 h suggesting that JcDNV might accumulate with time within midgut cells and then eliminated since its relative amount dropped by 24 h pi. At 48 h pi, a slight increase in tracheae, but not detected in hemocytes, suggested the initiation of viral replication. By 72 h pi, viral genome amplification was clearly observed in hemocytes and trachea and became exponential at 4 days pi (data not shown). No amplification was observed in midgut cells thus confirming that *Jc*DNV does not replicate in these cells. The quantification of the viral copy number allowed us to estimate *Jc*DNV infectivity, assimilating the number of viral genomes to viral particles per larva. Larvae were initially infected with 10^{11} vg, at 4 h pi we estimate that an average of 10^7 and 10^8 vg were found respectively in hemocytes and tracheae per larva while 2×10^6 vg were found within midgut cells. These results suggested that approximately 0.1% of viral particles efficiently crossed the midgut epithelium and reached these tissues. Interestingly, at 16 h pi, a relative higher amount of JcDNV was detected in midgut suggesting an accumulation within this tissue. At 24 h pi, an overall drop of *Jc*DNV was observed in all the tissues, suggesting that *Jc*DNV had entered a latency phase before the initiation of viral replication only detected in hemocytes and tracheal cells between 48 and 72 h pi. Since 10^5 and 10^6 vg were found per larva, respectively in hemocytes and tracheae, this suggested that 0.01% viral particles that crossed the midgut were actually infectious. In these conditions, the viral particle-to-infection ratio was roughly estimated at $1{:}10^5$ in tracheal cells and $1{:}10^6$ in hemocytes. Interestingly, a similar high *Jc*DNV particle-to-infection ratio had been estimated by a different method on Ld652 cell culture (Vendeville et al., 2009).

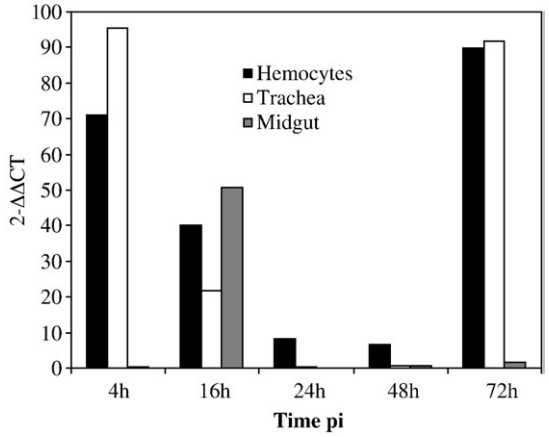

Fig. 3. Time course of JcDNV replication in *S. frugiperda*. Larvae were infected at L4 stage and DNA was extracted from hemocytes, trachea and midgut cells at various times pi and quantified with real time qPCR ($n=10$ larvae per tissue and per time point). Virus DNA was quantified using virus-specific primers and the ubiquitin gene was used to quantify cellular DNA. Values represent the mean ratio of viral/cellular DNA of 3 different experiments.

These results highlight the barrier function of the midgut resulting in a massive elimination of the *Jc*DNV input. Once in trachea or hemocytes, only 1% of *Jc*DNV particles were infectious suggesting that additional cellular barriers impaired infection and contribute, to a lesser extent, to the relative low efficiency of infection. Concerning the spreading of infection, the mechanism by which *Jc*DNV gained access to target tissues remained unclear. Systemic transmission to epidermis might occur through hemocytes and tracheae as already described for baculovirus infection (Engelhard et al., 1994).

JcDNV infection leads to hypoxia

Host death is a consequence of the disease caused, directly or not, by virus multiplication. Epidermic cells were highly replicative resulting in structural and functional alterations in the epidermis and tracheae. In particular, as the tracheal network transports and delivers oxygen to demanding tissues, its infection might have a broad systemic incidence and could lead to early pathologies.

We next analysed the structure of the tracheal network from L2 infected larvae late in infection. Curiously, we systematically observed that the tracheoles branching on the midgut, either dorsally or ventrally, displayed a tortuous morphology compared to stage-matched control larvae (Fig. 4A, 1–2 and 4–5). This phenotype was reminiscent of the tracheal overgrowth previously observed and attributed to oxygen deprivation (Jarecki et al., 1999; Wigglesworth, 1954). Phase contrast observation of these tracheae showed a cell enlargement, corresponding to the densonucleosis (Fig. 4A, 3 and 6). This defect, correlated with *Jc*DNV immuno-labelling, propagated with time, from the tip of these visceral tracheae to main branches (data not shown). This suggested that *Jc*DNV was transmitted with time from one cell to another, spreading infection in a directional way along the tracheal branches.

Since tracheal dysfunction would result in early default in delivering oxygen, we assessed for an oxidative stress in cells by measuring the total reactive oxygen species (ROS) generated at different times pi. We analysed ROS induction in visceral tracheae and in poorly replicative fat body cells, where cytopathies might be a secondary effect of infection. Because their size was easy to dissect, cohorts of L4 larvae were mock-infected or infected with 100 LD_{50}. At different times post infection, tracheae and fat body were dissected and cellular extracts were prepared from these two tissues to measure the ROS production with a fluorescent assay. Surprisingly, in tracheal cell extract, a significant ROS induction was observed early in infection, at one day pi (Fig. 4B, left panel), prior to viral replication (see Fig. 3C), and before any detectable sign of disease. Induction remained similar at day-two pi compared to stage-matched mock-infected larvae and decreased significantly at day-four pi, correlating with the *Jc*DNV amplification phase. In fat body cells (Fig. 4B, right panel), a relative higher ROS induction was also observed at day-one pi but then dropped at day-two and 4 pi. In both tissues, ROS induction decrease was correlated with the exponential phase of viral replication.

To corroborate oxygen deprivation, we next considered the larvae respiratory activity by measuring the relative oxygen consumption using an oxygraph apparatus. Two batches of six larvae, one batch of L2-infected larvae at 5-days pi and one batch of mock-infected larvae, were kept for 1 h in the two chambers of the oxygraph. The respective oxygen consumption of each batch was independently measured by two probes and normalised on the larval weight of each batch. As shown in Fig. 4C, oxygen consumption was significantly lower in 5 day infected larvae compared to the control larvae confirming that late in infection, the respiratory activity is significantly decreased in infected larvae.

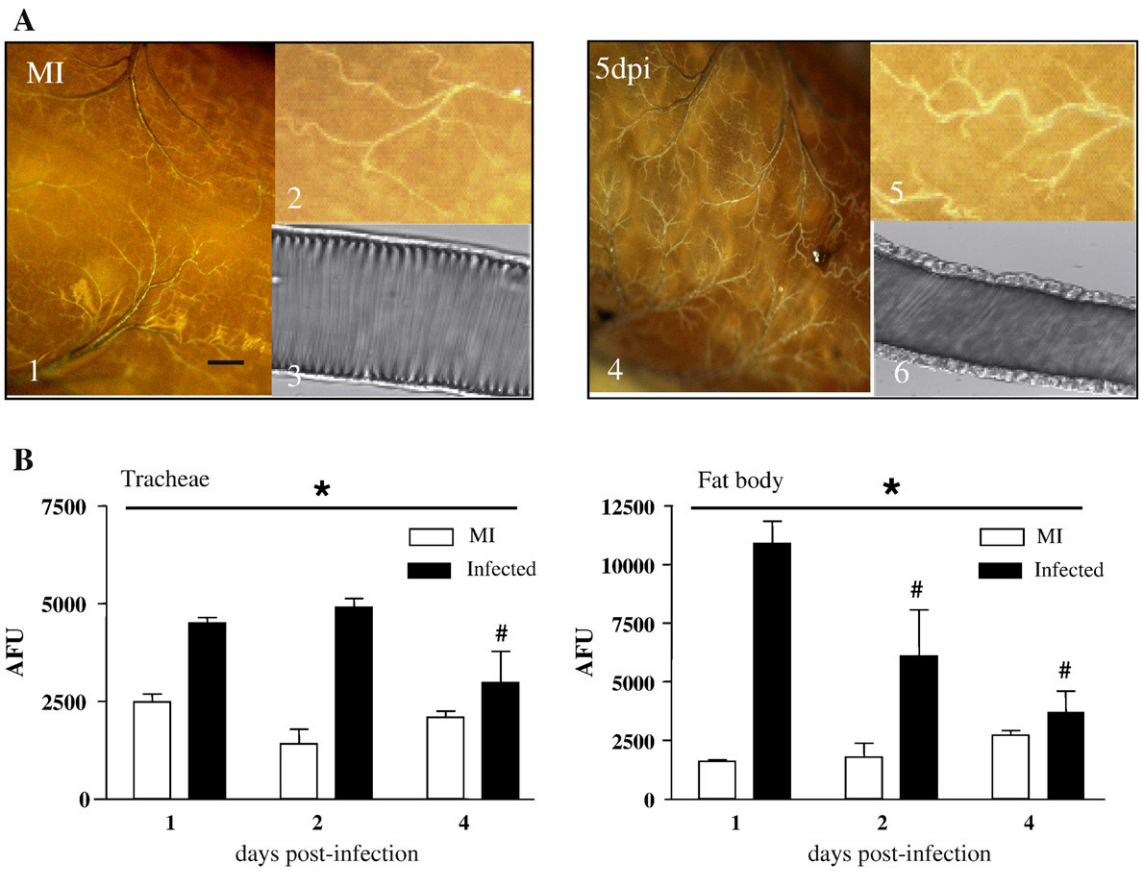

C

Conditions	Oxygen consumption activity (pmol O_2 s^{-1} g (f.w.)-1
MI	102.83 ± 23.42 (*a*)
*Jc*DNV	54.77 ± 11.64 (*b*)

Fig. 4. Effects of *Jc*DNV infection on *S. frugiperda* trachea structure and function. (A) Tracheal network branching on the midgut of mock-infected (1–2) or 5-day infected larvae (4–5). Trachea whole mount phase contrast observations (3–6). Scale bars, 5 mm (1–4), 0.2 mm (2–3; 5–6). (B) ROS detection in larvae infected at different times pi in tracheal cell extracts (left panel) and fat body cell extracts (right panel). Two-way ANOVA, $^{*}p<0.0001$ (mock-infected versus infected) and Bonferroni post hoc test $^{\#}p<0.0001$ (versus one day). (C) Measurement of oxygen consumption. Infected and mock-infected caterpillars were poured in the two sealed thermostated chambers (28 °C) of a high-resolution oxygraph to measure their respective oxygen consumption.

Discussion

In this work we first described the infection and pathogenesis of *S. frugiperda* larvae infected with a densovirus. How oral infection with a non-enveloped virus proceeds in insects is poorly documented, *Spodoptera* and *Jc*DNV provide a powerful model to study the infection process and the mechanisms underlying host range and specificity. The pathogenesis of *Jc*DNV infection is initiated after ingestion of contaminated food by the caterpillar. Results show that infection mostly depends on dose, time and larval instar as already observed for *Gm*DNV infections of its host, *G. melonella* (Boemare and Brès, 1969). Once ingested, *Jc*DNV small size might diffuse freely through the peritrophic membrane protecting midgut cells and whose pore size has been estimated between 21 and 29 nm in Lepidoptera (Martin and Barbehenn, 1997). Then, the success of *Jc*DNV oral infection depends on midgut cell recognition and entry. Although no replication occurs in those cells, virus entry and traffic are critical and the results presented here show that in *S. frugiperda*, crossing the midgut roughly eliminates 99.9% of *Jc*DNV, highlighting the barrier-to-infection function of this tissue. We estimate that 0.1% of the viral particles successfully cross the midgut epithelium and directly reach underlying tissues, among them tracheae and hemocytes, although visceral muscles surrounding the midgut, might be directly infected as well. How and when viral particles are transported to epidermis remained to be clarified. Epidermis is probably the higher replicative tissue as suggested by the viral pseudo-crystalline arrangements only observed in these cells. As a consequence of epidermal cells infection, molting is impaired 3–4 days pi corresponding to the exponential phase of viral replication. Considering this kinetic, it is likely that epidermis is a primary infected tissue. Interestingly, we could not detect *Jc*DNV in cell-free hemolymph at any time point tested, from 4 h to 3 days pi. *Jc*DNV might be transported by hemocytes and infect epidermis through cell-to-cell contact. It has been previously demonstrated that the tracheal system is the principal route for the systemic spread of the baculovirus within an insect (Engelhard et al., 1994; Haas-Stapleton et al., 2003). Our results highlight that diverse insect virus groups may use similar strategies to spread within a host. We can speculate that both hemocytes and tracheal cells may provide hiding places to escape host immune response.

The relative low efficiency of infection might be compensated by a very efficient *Jc*DNV replication, as suggested by the large sized viral populations generated in larvae. Since neither the midgut nor the fat

body replicates *Jc*DNV, their functions might be preserved and larvae continue to feed and grow until late in infection as we observed. We assume that viral reproduction might be boosted in a metabolically active and growing host; consequently transmission might be optimised as suggested by the natural epizootics described.

Our pathogenesis study suggests that tissues are directly or indirectly affected by *Jc*DNV replication and cellular injuries are very important determinants of the disease progression. We showed that organism's main physiological functions, molting and respiration are severely affected. At the cellular level this pathology is supported by the structural disorganisation of epidermal cells. One intriguing aspect of *Jc*DNV pathogenesis is the tracheal overgrowth. First described by Wigglesworth (1954), several works on insects showed the impact of hypoxia on tracheae proliferation and on developmental arrest (Harrison et al., 2006; Jarecki et al., 1999; Wingrove and O'Farrell, 1999). Hypoxia preceding the severe respiration defaults we observed, the tracheal overgrowth phenotype might result from hypoxic cell oxygen demand, through locally secreted signals as suggested by these previous works. Alternatively, tracheal cell overgrowth might be directly attributed to *Jc*DNV replication, *e.g.* by regulating signalling pathways leading to cell proliferation. Intriguingly, we found that ROS early induction occurred in tracheal cells before viral replication, suggesting that this signal is triggered by *Jc*DNV entry. ROS signalling is complex and may lead to cell proliferation or death. How tracheal cells deal with proliferative and death signals throughout the *Jc*DNV infection process is unknown. We cannot exclude that tracheal intrinsic ROS signalling might participate, early in infection, to the tracheal overgrowth. However ROS is also a potent antimicrobial agent, a reactive intermediate of oxygen generated, also in tracheae, during the melanisation reaction (Tang et al., 2008). We do not observe tracheal or epidermal melanisation, however melanisation is observed on the cuticle of infected larvae shortly before death. Whether ROS induction is a local humoral response to a microbial entry, this response might be blocked by *Jc*DNV products since no melanisation is associated. Interestingly, we found that late in infection, but before any sign of disease, ROS decreased in tracheal and fat body cells. This result supports the idea that ROS response might be controlled by infection products.

In summary, these results show that the pathogenesis of *Jc*DNV in an opportunistic host leads to severe defects in all the tissues with main physiological consequences. At the cellular level, these results highlight that early events of virus entry are crucial events controlling host range and tissue tropism. We need to understand these processes for a further use of densoviruses as biological control agents.

Materials and methods

Larvae and virus

S. frugiperda larvae were grown on a semi artificial diet at 24 °C under 12/12 h photoperiod. Under these conditions, *S. frugiperda* has 6 larval instars.

To prepare *Jc*DNV stock virus, 100 larvae were injected with JcDNV and then left to grow for 7–10 days on the diet. Dead larvae were collected and virus extraction and purification were performed on a renographine salt continuous density gradient and then dialysed as previously described (Jousset et al., 1990). Subsequently, virus was aliquoted and maintained at −20 °C until use. Viral concentration was estimated by quantitative PCR at 2.5×10^{14} viral genomes (vg)/ml. *Jc*DNV titre was determined on Ld 652 cells by the method developed by Li et al. (1996) since DNV infections do not produce cell lysis.

Lethal dose (LD) 50 and time to death for infected larvae

S. frugiperda newly molted larvae from L2 to L5 were starved before infections performed individually within tissue culture plates (24- to 6-wells depending on their size) by feeding with 1 mm^3 of diet contaminated with 1 µl of *Jc*DNV preparation. Cohorts of infected larvae (30 larvae per concentration point) were fed and time zero of infection was defined when food was eaten, feeding usually lasted for 15–30 min depending on the stage. Infected and control larvae were then fed with fresh food at 24 °C until death.

Analysis of the pathology

The pathology and tissue tropism were examined by dissecting larvae infected at various time post infection (pi) performed as described above. Tissues were fixed for 1 hour (h) in 4% paraformaldehyde (PFA) and then washed in conventional phosphate-buffer saline (PBS) pH 7. Total hemocytes were collected and fixed with 4% PFA for 20 min. For crysosections, midguts were included in OCT and frozen in liquid nitrogen. Four µm cryosections were realised with a Leica cryostat (2800E Frigocut, CM3050).

To evaluate midgut cells renewal, mock-infected or 5-day infected larvae were injected with 15 µg BrdU (Sigma) for 24 h; midguts were then dissected and fixed. Permeabilization was performed in PBS + Triton X-100 (PBT) 0.1%, tissues were incubated overnight with 1:1000 mouse Anti *Jc*DNV antibody, or anti-BrdU antibody (Sigma), washed with PBS and incubated for 1 h with 1:500 alexa-594 anti mouse antibody or alexa-488 anti mouse antibody (Invitrogen). Tissues were whole mounted with Prolong (Invitrogene) on coverslips for microscopic observation.

Semi-thin and ultrathin sections were obtained by first fixing the tissues in 2% glutaraldehyde–0.1 M cacodylate (pH 7.4) for 1 h at 4 °C then post fixed for 1 h in 2% osmium tetroxide in cacodylated buffer. Following dehydration in graded series of ethanol solutions, samples were embedded into Epon resin. Sections were cut with a diamond knife in an LKB ultramicrotome. Semi-thin sections were mounted on coverslips and stained with toluidine blue, whereas ultrathin sections were mounted on copper grids, stained with uranyl acetate and lead citrate and observed with a Zeiss EM10CR electron microscope at 80 kV.

Viral DNA quantification

To determine the concentration of DNA-containing particles, we performed real time quantitative PCR. Total DNA was extracted between 4 h and 4 days pi from midgut cells, hemocytes and tracheal cells of L4 larvae whose size facilitates the dissection. Hemocytes were collected as described in Pech et al. (1994) by bleeding 10 mock-infected or infected L4 per time point. Cells were collected by 5 min centrifugation at 3000 rpm. The pellet was washed in PBS and then treated with DNA extraction buffer containing 15 mg/ml of proteinase K for 3 h at 37 °C before phenol extraction and precipitation. Visceral tracheae branching on the midgut were collected from different 10 L4 larvae cohorts and crushed before DNA extraction. DNA samples were recovered in 50 µl of water. Similarly, midguts from 10 L4 larvae were thoroughly washed and left for 30 min in collagenase-containing PBS (1 mg/ml, Sigma) to separate midgut cells from basal lamina and isolate them before DNA extraction. Viral Forward (5′-GGAGGAGGCAACACTTCAGG-3′) and Reverse (5′-TCTGCCATGGAATTTCAGCC-3′) primers were designed with the Primer Express® software (Applied Biosystem) optimised for the ABI prism 7000 Sequence detection system (SDS). A fragment was amplified from position 1710 to 1911 of the viral genome located within the viral ORF1 encoding the Viral Protein 4 (VP4), the major capsid protein. The ubiquitin gene was used as control gene to normalize DNA quantity between samples and experiments, the primers were designed from *S. frugiperda* ubiquitin cDNA sequence (Barat-Houari et al., 2006) Forward (ACTTGTGGCCCGCATACACT) and Reverse (GGATCGGCACAATAAATGGG). The reaction was carried out using platinum SYBR Green qPCR super mix kit (Invitrogen).

Fluorescent PCR amplicons were detected using the ABI PRISM 7000® apparatus (Applied Biosystems) using 96-well microtiter plates in a final volume of 25 µl under the following conditions: 50 °C for 2 min, 95 °C for 2 min, 40 cycles of 95 °C for 15 s and 60 °C for 30 s. For each quantitative PCR analysis 5 µl of diluted DNA was deposited in triplicates. A standard curve was generated after 40 cycles of PCR run using 7 serial tenfold dilutions of purified viral DNA. The linear range was obtained over 7 orders of magnitude. Data from two biological replicates, 3 technical replicates and 2 plates permutation were analysed by the ΔΔCt method (Schmittgen and Livak, 2008).

The viral standard curve was obtained using 7 serial tenfold dilutions of the purified viral DNA. The linear range was obtained from 1.25×10^3 to 1.25×10^9 copies of viral genome.

ROS and respiration assay

ROS production was evaluated in trachea and fat body. Briefly, tissues from 10 larvae were harvested and homogenized with a dounce homogenizer in 50–100 µl ice-cold phosphate buffer (8 mM). Homogenates were then disrupted by three freeze–thaw cycles in liquid nitrogen and an aliquot was used to determine protein concentration by Bradford assay.

Homogenates (25 µg) were incubated with 50 µM dichlorodihydrofluorescein diacetate (Invitrogen) and phosphate buffer at 37 °C, and ROS production was monitored for 60 min in a 96-well plate. ROS production was directly proportional to the fluorescence emission (525 nm) measured with a microplate fluorimeter (Synergy 2, Biotek Instruments). Results were expressed as arbitrary fluorescent units (AFU).

Measurement of oxygen consumption

Two batches of 6 caterpillars, 5-day infected and mock-infected controls were placed in the two sealed thermostated chambers (28 °C) of a high-resolution oxygraph (oxygraph-2k, Oroboros, Austria). After a 5 min equilibration period, the oxygen consumption rate (JO) was measured in the normoxic region (oxygen concentration ranging from 100 to 230 µM or between 3.75 and 7.5 mg of O_2 L^{-1}) in steady-state flux conditions as previously described (Gnaiger et al., 1995). Data were recorded at 1 s intervals (Datlab Acquisition software, Oroboros, Austria). Each experiment lasted less than 10 min. Oxygen concentration was corrected for the response time of the oxygen sensor as described by Gnaiger et al. (1995), after calibration with blank controls as described by Haller et al. (1994).

Acknowledgments

This paper is dedicated to the memory of Gérard Devauchelle. We are grateful to C. Gibard and M. Jambard for their great help in providing all the larvae we need and to M. Brehelin for helping us to determine hemocytes. Special thanks go to M. Bergoin for all the very helpful discussions and to A.-S. Gosselin and A. Perrin for their critical reading of the manuscript. We warmly thank C. Ripoll (Histology Facility, INM Montpellier), V. Diakou (MRI, Montpellier), and the TEM facility (UM2, Montpellier) for their technical support.

References

Abd-Alla, A., Jousset, F.X., Li, Y., Fediere, G., Cousserans, F., Bergoin, M., 2004. NS-3 protein of the *Junonia coenia* densovirus is essential for viral DNA replication in an Ld 652 cell line and *Spodoptera littoralis* larvae. J. Virol. 78 (2), 790–797.

Barat-Houari, M., Hilliou, F., Jousset, F.X., Sofer, L., Deleury, E., Rocher, J., Ravallec, M., Galibert, L., Delobel, P., Feyereisen, R., Fournier, P., Volkoff, A.N., 2006. Gene expression profiling of *Spodoptera frugiperda* hemocytes and fat body using cDNA microarray reveals polydnavirus-associated variations in lepidopteran host genes transcript levels. BMC Genomics 7, 160.

Bergoin, M., Bres, N., 1968. Lesions tissulaires chez la larve du lepidoptère Galleria mellonela L. atteinte du virus de la densonucleosie. Bull. Apicole 11, 5.

Bergoin, M., Tijssen, P., 2008. Parvoviruses of arthropods. In: Mahy, B.W.J., VanRegenmortel, M.H.V. (Eds.), Encyclopedia of Virology, Vol. 5. Elsevier, Oxford, pp. 76–85.

Boemare, N., Brès, N., 1969. Le dévelopment du virus de la densonucleose au cours de la metamorphose de son hôte, *Galleria mellonella* L. (Lepidoptera). Ann. Zool. Ecol. anim. 1 (3), 309–320.

Carlson, J., Suchman, E., Buchatsky, L., 2006. Densoviruses for control and genetic manipulation of mosquitoes. Adv. Virus Res. 68, 361–392.

Engelhard, E.K., Kam-Morgan, L.N., Washburn, J.O., Volkman, L.E., 1994. The insect tracheal system: a conduit for the systemic spread of *Autographa californica* M nuclear polyhedrosis virus. Proc. Natl. Acad. Sci. U. S. A. 91 (8), 3224–3227.

Fediere, G., El-Far, M., Li, Y., Bergoin, M., Tijssen, P., 2004. Expression strategy of densonucleosis virus from *Mythimna loreyi*. Virology 320 (1), 181–189.

Gnaiger, E., Steinlechner-Maran, R., Mendez, G., Eberl, T., Margreiter, R., 1995. Control of mitochondrial and cellular respiration by oxygen. J. Bioenerg. Biomembr. 27 (6), 583–596.

Haas-Stapleton, E.J., Washburn, J.O., Volkman, L.E., 2003. Pathogenesis of *Autographa californica* M nucleopolyhedrovirus in fifth instar *Spodoptera frugiperda*. J. Gen. Virol. 84, 2033–2040.

Haller, T., Ortner, M., Gnaiger, E., 1994. A respirometer for investigating oxidative cell metabolism: toward optimization of respiratory studies. Anal. Biochem. 218 (2), 338–342.

Harrison, J., Frazier, M.R., Henry, J.R., Kaiser, A., Klok, C.J., Rascon, B., 2006. Responses of terrestrial insects to hypoxia or hyperoxia. Respir. Physiol. Neurobiol. 154 (1–2), 4–17.

Hu, Y., Zheng, J., Iizuka, T., Bando, H., 1994. A densovirus newly isolated from the smoky-brown cockroach *Periplaneta fuliginosa*. Arch. Virol. 138 (3–4), 365–372.

Jarecki, J., Johnson, E., Krasnow, M.A., 1999. Oxygen regulation of airway branching in *Drosophila* is mediated by branchless FGF. Cell 99 (2), 211–220.

Jousset, F.X., Jourdan, M., Compagnon, B., Mialhe, E., Veyrunes, J.C., Bergoin, M., 1990. Restriction maps and sequence homologies of two densovirus genomes. J. Gen. Virol. 71, 2463–2466.

Li, Y., Jousset, F.X., Giraud, C., Rolling, F., Quiot, J.M., Bergoin, M., 1996. A titration procedure of the *Junonia coenia* densovirus and quantitation of transfection by its cloned genomic DNA in four lepidopteran cell lines. J. Virol. Methods 57 (1), 47–60.

Martin, M.M., Barbehenn, R.V., 1997. Permeability of the peritrophic envelopes of herbivorous insects to dextran sulfate: a test of the polyanion exclusion hypothesis. J. Insect. Physiol. 43 (3), 243–249.

Meynadier, G., Vago, C., Plantevin, G., Atger, P., 1964. Virose d'un type inhabituel chez le lépidoptère *Galleria mellonella* L. Rev. Zool. Agri. Appl. 63, 207–208.

O'Neill, S.L., Kittayapong, P., Braig, H.R., Andreadis, T.G., Gonzalez, J.P., Tesh, R.B., 1995. Insect densoviruses may be widespread in mosquito cell lines. J. Gen. Virol. 76, 2067–2074.

Pech, L.L., Trudeau, D., Strand, M.R., 1994. Separation and behavior in vitro of hemocytes from the moth, *Pseudoplusia includens*. Cell Tissue Res. 277 (1), 159–167.

Ren, X., Hoiczyk, E., Rasgon, J.L., 2008. Viral paratransgenesis in the malaria vector *Anopheles gambiae*. PLoS Pathog. 4 (8), e1000135.

Rivers, C.F., Longworth, J.F., 1972. A nonoccluded virus of *Junonia coenia* (Nymphalidae: Lepidoptera). J. Invertebr. Pathol. 20, 369–370.

Schmittgen, T.D., Livak, K.J., 2008. Analyzing real-time PCR data by the comparative C (T) method. Nat. Protoc. 3 (6), 1101–1108.

Tang, H., Kambris, Z., Lemaitre, B., Hashimoto, C., 2008. A serpin that regulates immune melanization in the respiratory system of *Drosophila*. Dev. Cell 15 (4), 617–626.

van Munster, M., Dullemans, A.M., Verbeek, M., van den Heuvel, J.F., Reinbold, C., Brault, V., Clerivet, A., van der Wilk, F., 2003. Characterization of a new densovirus infecting the green peach aphid *Myzus persicae*. J. Invertebr. Pathol. 84 (1), 6–14.

Vendeville, A., Ravallec, M., Jousset, F.X., Devise, M., Mutuel, D., Lopez-Ferber, M., Fournier, P., Dupressoir, T., Ogliastro, M., 2009. Densovirus infectious pathway requires clathrin-mediated endocytosis followed by trafficking to the nucleus. J. Virol. 83 (9), 4678–4689.

Wigglesworth, V.B., 1954. Growth and regeneration in the tracheal system of an insect, *Rhodnius prolixus* (Hemiptera). J. Microsc. Sci. 95, 115–137.

Wingrove, J.A., O'Farrell, P.H., 1999. Nitric oxide contributes to behavioral, cellular, and developmental responses to low oxygen in *Drosophila*. Cell 98 (1), 105–114.